Nano Research
DOI 10.1007/s12274-014-0673-y
Research Article
ISSN 1998-0124
CN 11-5974/O4

MoS_2-wrapped silicon nanowires for photoelectrochemical water reduction

Liming Zhang[1,†,§], Chong Liu[1,§], Andrew Barnabas Wong[1,4], Joaquin Resasco[2], and Peidong Yang[1,3,4] (✉)

Nano Res., **Just Accepted Manuscript** • DOI: 10.1007/s12274-014-0673-y
http://www.thenanoresearch.com on December 2 2014

Just Accepted

TSINGHUA UNIVERSITY PRESS Springer

Template for Preparation of Manuscripts for *Nano Research*

This template is to be used for preparing manuscripts for submission to *Nano Research*. Use of this template will save time in the review and production processes and will expedite publication. However, use of the template is not a requirement of submission. Do not modify the template in any way (delete spaces, modify font size/line height, etc.). If you need more detailed information about the preparation and submission of a manuscript to Nano Research, please see the latest version of the Instructions for Authors at http://www.thenanoresearch.com/.

TABLE OF CONTENTS (TOC)

Authors are required to submit a graphic entry for the Table of Contents (TOC) in conjunction with the manuscript title. This graphic should capture the readers' attention and give readers a visual impression of the essence of the paper. Labels, formulae, or numbers within the graphic must be legible at publication size. Tables or spectra are not acceptable. Color graphics are highly encouraged. The resolution of the figure should be at least 600 dpi. The size should be at least 50 mm × 80 mm with a rectangular shape (ideally, the ratio of height to width should be less than 1 and larger than 5/8). One to two sentences should be written below the figure to summarize the paper. To create the TOC, please insert your image in the template box below. Fonts, size, and spaces should not be changed.

MoS_2-wrapped silicon nanowires for photoelectro-chemical water reduction

Liming Zhang, Chong Liu, Andrew Barnabas Wong, Joaquin Resasco, and Peidong Yang*

University of California, Berkeley, United States

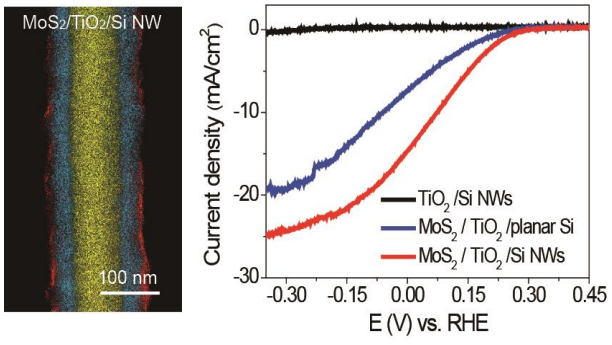

Silicon (Si) NW arrays were employed as a model photocathode system for MoS_2 wrapping, and their solar-driven HER activity was evaluated. The photocathode is comprised of a well-defined $MoS_2/TiO_2/Si$ coaxial NW heterostructure, which yielded photocurrent density up to 15 mA/cm^2 at 0 V vs. the reversible hydrogen electrode (RHE) with good stability under operating conditions.

Nano Research
DOI (automatically inserted by the publisher)
Research Article
ISSN 1998-0124
CN 11-5974/O4

MoS_2-wrapped silicon nanowires for photoelectrochemical water reduction

Liming Zhang[1,†,§], Chong Liu[1,§], Andrew Barnabas Wong[1,4], Joaquin Resasco[2], and Peidong Yang[1,3,4] (✉)

[1]*Department of Chemistry,* [2]*Department of Chemical Engineering and* [3]*Department of Materials Science and Engineering, University of California, Berkeley, CA 94720, United States*
[4]*Materials Science Division, Lawrence Berkeley National Laboratory, Berkeley, CA 94720, United States*
[†]*Present address: Department of Materials Science and Engineering, Stanford University, Stanford, CA 94305, United States*
[§]*These authors contributed equally to this work.*

Received: day month year
Revised: day month year
Accepted: day month year (automatically inserted by the publisher)

KEYWORDS

MoS_2, Si nanowire array, coaxial heterostructure, photoelectrochemistry, hydrogen evolution reaction (HER)

ABSTRACT

Integration of molybdenum disulfide (MoS_2) onto high surface area photocathodes is highly desired to minimize the overpotential for solar-powered hydrogen evolution reaction (HER). Semiconductor nanowires (NWs) are beneficial for use in photoelectrochemistry because of a large electrochemically available surface area and their inherent ability to decouple light absorption and the transport of minority carriers. Here, silicon (Si) NW arrays were employed as a model photocathode system for MoS_2 wrapping, and their solar-driven HER activity was evaluated. The photocathode is comprised of a well-defined $MoS_2/TiO_2/Si$ coaxial NW heterostructure, which yielded photocurrent density up to 15 mA/cm^2 at 0 V vs. the reversible hydrogen electrode (RHE) with good stability under operating conditions. This work reveals that earth-abundant electrocatalysts coupled with high-surface area NW electrodes can provide performance comparable to noble-metal catalysts for photocathodic hydrogen evolution.

Address correspondence to p_yang@berkeley.edu

1 Introduction

The vision of utilization of hydrogen as a future energy source requires a sustainable, highly efficient, and cost-effective production method [1]. To use renewable energy to produce hydrogen fuel, solar-driven water splitting is one of the most promising approaches [2, 3]. Effective photelectrochemical (PEC) water splitting devices must be able to absorb a large fraction of incident sunlight, generate high photocurrent with sufficient photovoltage, and exhibit long-term stability. One challenge in designing such a device is to reduce the reaction overpotential, by increasing the reaction kinetics on the surface. While existing noble metal catalysts, such as Pt, are highly active at catalyzing the hydrogen evolution reaction (HER) [4, 5], the high cost of these materials limits the economic viability of their use for hydrogen production. The intensive search for earth-abundant, inexpensive, and nontoxic catalysts with comparable performance for the HER has led to significant progress in the development of new catalysts, including metal alloys [6, 7], nitrides [8], borides [9], carbides [9, 10], chalcogenides [11-16], and phosphides [17]. In particular, metal chalcogenides, such as molybdenum sulfide (MoS_x), are an exciting group of HER catalysts that exhibit promising activity in both crystalline and amorphous forms, as well as in the form of grafted molecular clusters [11, 12, 18-20]. Despite the considerable efforts dedicated to investigating and optimizing the catalytic activity of various MoS_x materials, the effective integration of MoS_x onto photocathodes is still a challenge. To achieve high geometric area-normalized HER activity, it is necessary to carefully engineer MoS_x functional nanostructures to maximize the density of active sites, which have been identified both theoretically [21, 22] and experimentally [11, 12, 23, 24] to be the uncoordinated sulfur edge sites.

High-surface area photoelectrodes, such as semiconductor nanowire (NW) arrays, are attractive because of their large semiconductor/electrolyte interfacial area, enhanced light scattering effect, and efficient transport of charge carriers [25-27]. Silicon (Si), with bandgap of 1.12 eV, is a promising candidate as a light-absorber due to its relatively low cost, excellent carrier transport properties, and suitable band edge with respect to HER potential [27]. As atomically thin MoS_2 has limited light absorption, the successful integration of MoS_2 with semiconductor NWs constitutes an ideal system for PEC hydrogen production.

In this work, using a p-Si NW array as scaffold, a well-defined MoS_2/TiO_2/Si NW integrated coaxial heterostructure was constructed as a model photocathode system for PEC hydrogen generation. Multilayer MoS_2 with a small domain size of ~10 nm was uniformly wrapped on the surface of the NWs, exposing a high density of active uncoordinated edge sites. An onset of photocurrent at ~ 0.30 V vs. the reversible hydrogen electrode (RHE), together with a short-circuit current density of 15 mA/cm^2 under simulated 1 sun illumination was achieved. Additionally, this functional device exhibits good stability under operating conditions. This system demonstrates the principle that earth-abundant electrocatalysts coupled with high-surface area NW electrodes can provide performance comparable to noble-metal catalysts for photocathodic hydrogen evolution. This principle could serve as a guide for future studies in the field of solar-powered chemical fuel production, by offering an additional dimension for device engineering through the benefits of the NW morphology.

2 Results and Discussion

Metal oxide overlayers can assist to preserve the photo-response of Si [28], consequently for our study, Si/TiO_2 core-shell structures were prepared

via atomic layer deposition (ALD) of 30 nm of crystalline TiO_2 on the NW surface at 573 K. The MoS_2 layer was synthesized by thermolysis of ammonium tetrathiomolybdate [$(NH_4)_2MoS_4$] at low temperature [29, 30]. $(NH_4)_2MoS_4$ was dissolved in an organic solvent and drop-casted onto the NW surface [additional details are provided in the Electronic Supplementary Materials (ESM)]. After drop-casting, the coated NWs were annealed at 573~673 K in a N_2/H_2 (80/20 sccm) atmosphere at ambient pressure to form MoS_2.

A single TiO_2/Si NW wrapped with MoS_2 was characterized by high-angle annular dark field (HAADF) imaging (Figure 1a). The MoS_2 and TiO_2 shells appear brighter as Ti and Mo atoms located in the shell have a higher atomic number than the Si atoms in the core. High-resolution transmission electron microscopy (HRTEM) revealed multiple layers of MoS_2 on the NW surface, as evidenced by the lattice fringes with a spacing of 0.62 nm, in agreement with the expected MoS_2 interlayer distance of 0.614 nm (Figure 1b) [31, 32]. The crystallinity of MoS_2 highly depends on the annealing temperature, with increasing temperature resulting in higher crystallinity (Figure S1 in the ESM). Although the surface is mostly covered with MoS_2 basal planes, the domain size is smaller than 10 nm and crystal edges of MoS_2 are evidently abundant (indicated by the red arrows in Figure 1b). Relative to MoS_2 coated on planar electrode surfaces [18, 33], this core-shell structure exposes more MoS_2 edges because of the large surface area afforded by the NW morphology. Further analysis of the elemental distribution was obtained from energy dispersive X-ray spectroscopy (EDS) mapping. The elemental map shows a homogenous distribution of Si in the core (Figure 1c), Ti in the inner shell (Figure 1d), and a thin layer of Mo in the outer shell (Figure 1e). The combined elemental mapping in Figure 1f demonstrates a well-defined coaxial heterostructure of MoS_2/TiO_2/Si along a single NW. The uniform coating of MoS_2 distributes the solar-generated electron flux evenly along the semiconductor light-absorber. The effective utilization of the high surface area of the NW decreases the surface flux of electrons, leading to a reduced HER kinetic overpotential.

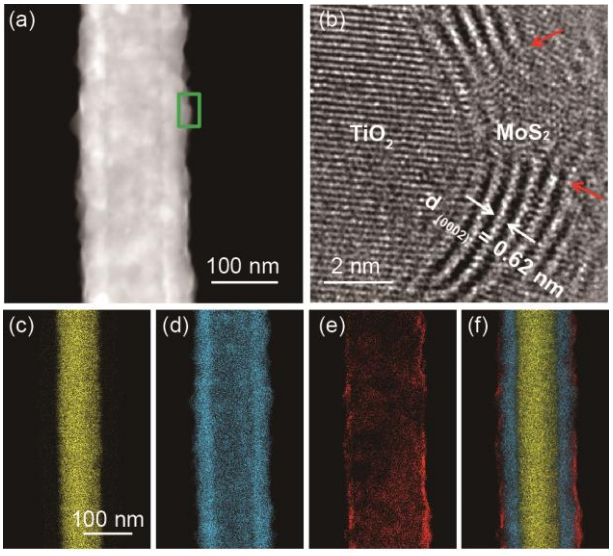

Figure 1 (a) HAADF image of the MoS_2/TiO_2/Si coaxial structure on a single NW. (b) HRTEM image taken at the MoS_2/TiO_2 interface as shown in the green box of (a). The lattice fringes show a spacing of 0.62 nm between adjacent layers, which is in agreement with the expected MoS_2 interlayer distance. The red arrows indicate the edge of a MoS_2 cluster where HER-active MoS_2 edge sites are likely exposed on the NW surface. (c-f) EDS elemental mapping along a single NW, which shows the elemental distribution of Si (c), Ti (d), Mo (e), and the combined signal of Mo/Ti/Si(f), respectively, demonstrating the well-defined integrated coaxial heterotructure of MoS_2/TiO_2/Si NW.

Additional characterization was performed to understand the nature of the synthesized MoS_2, from which deeper insight into the performance may be gained. Thermolysis of $(NH_4)_2MoS_4$ at low temperature in the presence of H_2 will result in the conversion initially to MoS_3 and finally to MoS_2 [29]. X-ray photoelectron spectroscopy (XPS) (Figure 2) and Raman spectroscopy (Figure S2 in the ESM) were used to investigate the chemical states of Mo and S before and after annealing. The binding energy of the Mo $3d_{5/2}$ photoelectron peak remained

constant (229.2 eV) before and after annealing, indicating a 4+ oxidation state for Mo [13]. The S 2p region of MoS_x before annealing shows two doublets, consistent with that seen for MoS_3 amorphous catalysts [13]. The doublet at lower binding energy (162.2 and 163.4 eV) is attributed to S^{2-} at the basal plane, characteristic of MoS_2. The doublet at higher binding energy (163.8 and 165.0 eV) is attributed to S_2^{2-} at the bridge sites. After annealing, only the doublet at lower binding energy corresponding to MoS_2 is observed. These results demonstrate that this low temperature annealing process is a simple method for the synthesis of stoichiometric MoS_2 catalysts with small domain sizes and uniform coverage, even on highly corrugated surfaces.

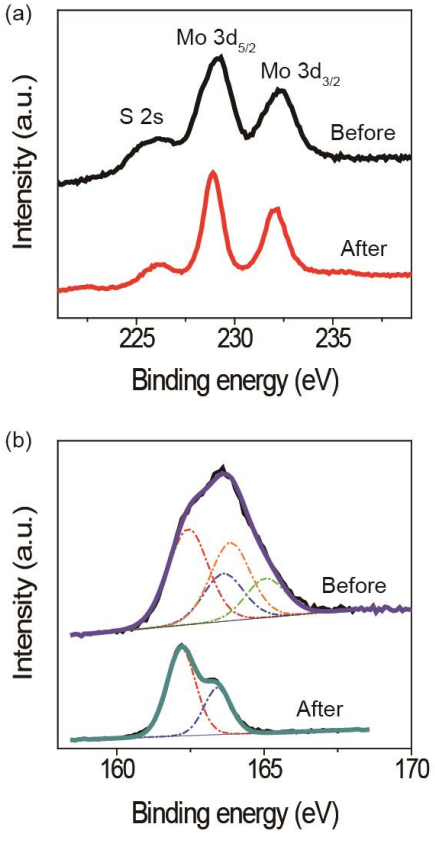

Figure 2 XPS characterization of Mo (a) and S (b) signal in the MoS_x cocatalyst before and after annealing. The Mo 3d region shows the Mo oxidation state is 4+ before and after annealing while the S 2p region shows a transition from MoS_3 to MoS_2.

The electrocatalytic performance of MoS_2 layers was first evaluated using planar p^+-Si substrate as an electrode. Different volumes of precursor solution, corresponding to different loadings of the MoS_2 cocatalyst, were drop-casted onto the electrode surface, followed by annealing at 673 K in a N_2/H_2 atmosphere at ambient pressure. The TiO_2 interlayer was required to achieve stable current; otherwise, the underlying Si will be gradually oxidized, leading to a decrease in activity (Figure S3 in the ESM). The catalytic performance was measured using iR-compensated linear scan voltammetry in 0.5 M H_2SO_4 electrolyte in a three-electrode configuration. Onset of cathodic current was observed at approximately -0.20 V vs. the reversible hydrogen electrode (RHE) (Figure 3a). The cathodic current increased with increasing loading of MoS_2 and exhibited a Tafel slope of 75~84 mV per decade (Figure 3b). The apparent exchange current densities j_0 were obtained from the Tafel plots and are summarized in the Supporting Information (Table S1 in the ESM). The Tafel slope observed here compares favorably with MoS_2 synthesized by chemical vapor deposition (CVD) on glassy carbon electrodes [18, 34]. After evaluating the dependence of HER activity on the MoS_2 loading density, the optimal condition was applied to the NW photoelectrodes for subsequent PEC investigation.

To evaluate the impact of MoS_2 cocatalyst deposition on the solar-to-hydrogen activity of the Si NW photocathodes, PEC measurements were performed under the same conditions as the electrochemical measurements described above. A well-defined high-surface area Si NW arrays electrode was fabricated via deep reactive ion etching (DRIE) (experimental details are provided in the ESM). The scanning electron micrographs are shown in Figure 3c-d. The etched NW arrays are approximately 30 μm in length and 800 nm in diameter, and are arranged on a square lattice with periodicity of 2 μm. In order to achieve a positive

photovoltage, a heavily doped n^+ emitter layer was diffused into the surface region of Si NWs via rapid temperature annealing at 1173 K for 3 min, using arsenic (As) as an n-type dopant. Following the procedure outlined above, a $MoS_2/TiO_2/n^+p$-Si NW coaxial heterostructure was created from the Si NW array. For comparison, $Pt/TiO_2/n^+p$-Si NW was also fabricated by sputtering Pt nanoparticles onto the NW surface (Figure S4 in the ESM). The PEC performance of these photoelectrodes was tested under identical conditions, using 100 mW/cm^2 simulated AM 1.5G irradiation. Figure 3e shows the activity comparison of Si photocathodes before and after deposition of MoS_2. Si NW arrays exhibit nearly no photo-activity in the absence of a cocatalyst. When MoS_2 was deposited onto the NW surface, the onset of photocurrent shifted substantially to a more positive potential (~ 0.30V vs. RHE), only 100 mV cathodic of the Pt nanoparticle decorated electrode. For the affordable application of overall water splitting by coupling of dual light absorbers, a current density on the order of 10 mA/cm^2 is necessary [20]. The MoS_2 layers wrapped Si NW array photocathode provides a current density of ~15 mA/cm^2 at 0 V vs. RHE, Indicating that this photocathode can affordable integrated water-splitting system.

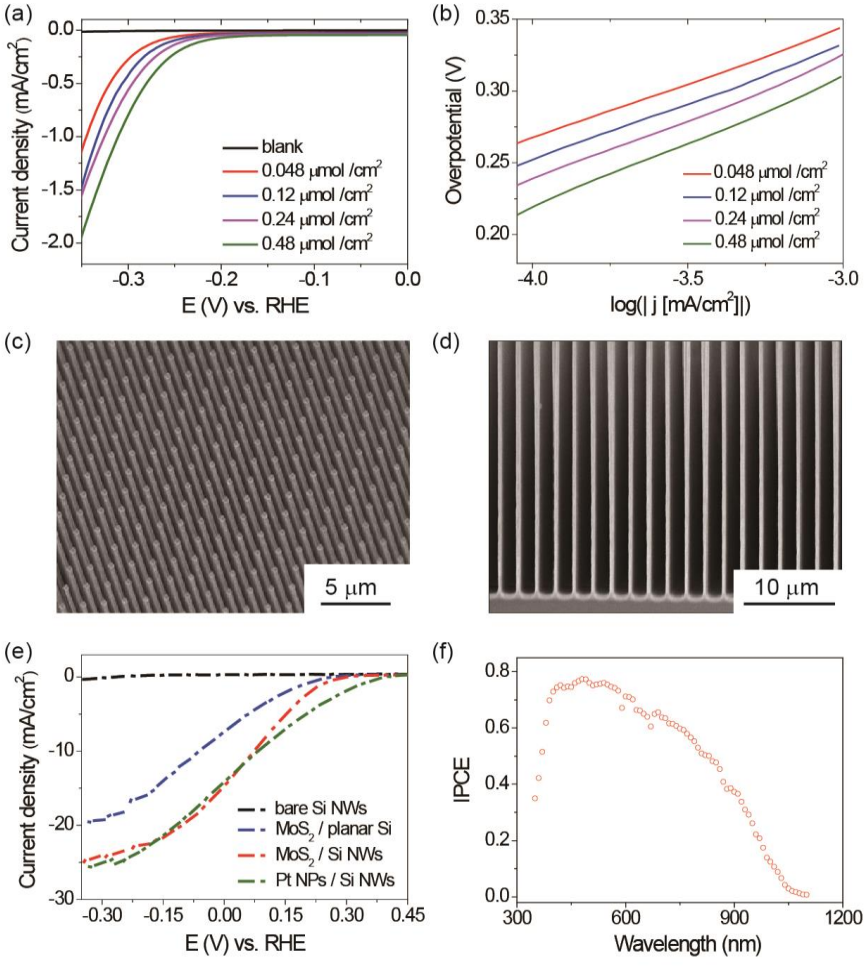

Figure 3 (a-b) Electrochemical performance of MoS_2 catalysts in 0.5 M H_2SO_4. (a) Linear sweep voltammograms and (b) Tafel plots for TiO_2-coated p^+-Si planar surface with different MoS_2 loadings. (c) 45° tilt and (d) cross-sectional SEM images of as-grown Si NW arrays. (e) Comparison of HER performance (under 100 mW/cm^2 simulated AM 1.5G irradiation) of Si NW array photocathodes coated with MoS_2 to an MoS_2 coated planar Si substrate, and a Si NW array loaded with Pt nanoparticles. (f) Spectral response [incident photon to current conversion efficiency (IPCE)] of Si NW arrays after coating with MoS_2 layers.

To study the impact of NW surface area on the required catalytic activity, an equal loading of MoS_2 was deposited on the surface of a planar TiO_2/n^+p-Si electrode. As shown in Figure 3e, the photo-activity was substantially improved in the Si NW array, indicating that increasing the surface area will decrease the surface flux of electrons, leading to a lower requirement for the catalytic activity on the surface. Figure 3f shows the typical spectral response for MoS_2/TiO_2/n^+p-Si NWs (experimental details are provided in the ESM). The external quantum efficiency reaches a maximum at 500 nm, consistent with the external quantum efficiency observed for Si wires coated with a thin layer of Pt nanoparticles [4]. The maximum external quantum efficiency is larger than 0.75, ~25% higher than previously reported for Ni-Mo coated Si wire arrays [7].

Another important criterion for PEC energy conversion is the long-term stability of the photoelectrode under operating conditions. The short-term stability of the coaxial MoS_2/TiO_2/Si NW structure and its faradaic efficiency for hydrogen reduction were evaluated by chronoamperometry. The potential of the photocathode was held at -0.33 V vs. RHE under 100 mW/cm^2 simulated AM 1.5 G irradiation, and both the photocurrent and hydrogen gas concentration in the Ar carrier gas were monitored. Bubbles were continuously evolved from photocathode, and the accumulation and release of these bubbles led to the observed variations in photocurrent over the duration of the measurement. The photocurrent of the coaxial MoS_2/TiO_2/Si NW structure remained at approximately 21 mA/cm^2 for 75 min without degradation (Figure 4), and the faradaic efficiency for hydrogen evolution to H_2 was found to be ~100% (more details are provided in the ESM and Figure S5). This result shows that the coaxial MoS_2/TiO_2/Si NWs are stable and are indeed reducing water into H_2.

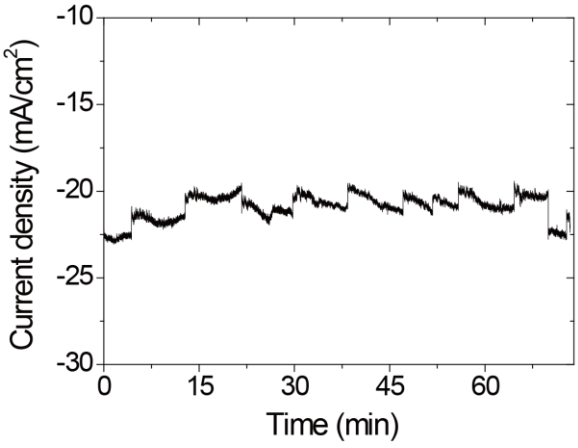

Figure 4 Stability test of MoS_2 wrapped Si NW array. Current vs. time during the controlled potential photoelectrolysis under 100 mW/cm^2 simulated AM 1.5G irradiation at -0.33 V vs. RHE.

3 Conclusions

In brief, this work shows the feasibility of functionalizing a Si NW array photocathode with a MoS_2 cocatalyst to drive solar hydrogen production. The exploration of the earth-abundant catalyst MoS_2, and its application to high surface area Si NW array electrodes establishes a general strategy to replace precious-metal cocatalysts for efficient and affordable solar-to-fuel application at a large scale.

Acknowledgements

This work was supported by the Director, Office of Science, Office of Basic Energy Sciences, Materials Science and Engineering Division, U.S. Department of Energy under Contract No. DE-AC02-05CH11231 (P-Chem). J.R. gratefully acknowledges the support of the National Science Foundation Graduate Research Fellowship Program (NSF GRFP) under Grant No. DGE-0802270.

Electronic Supplementary Material: Experimental details, additional TEM, Raman data, stability measurement, and calculations of electrochemical performance. This material is available in the online version of this article at http://dx.doi.org/10.1007/s12274-***-****-*

References

[1] Turner, J.A. Sustainable hydrogen production. *Science* **2004**, 305, 972-974.

[2] Walter, M.G.; Warren, E.L.; McKone, J.R.; Boettcher, S.W.; Mi, Q.; Santori, E.A.; Lewis, N.S. Solar water splitting cells. *Chem. Rev.* **2010**, 110, 6446-6473.

[3] Lewis, N.S.; Nocera, D.G. Powering the planet: Chemical challenges in solar energy utilization. *Proc. Natl. Acad. Sci.U.S.A.* **2006**, 103, 15729-15735.

[4] Boettcher, S. W.; Warren, E. L.; Putnam, M. C.; Santori, E. A.; Turner-Evans, D.; Kelzenberg, M. D.; Walter, M. G.; McKone, J. R.; Brunschwig, B. S.; Atwater, H. A.; Lewis, N. S. Photoelectrochemical hydrogen evolution using Si microwire arrays. *J. Am. Chem. Soc.* **2011**,133, 1216-1219.

[5] Dasgupta, N. P.; Liu, C.; Andrews, S.; Prinz, F. B.; Yang, P. Atomic layer deposition of platinum catalysts on nanowire surfaces for photoelectrochemical water reduction. *J. Am. Chem. Soc.* **2013**, 135, 12932-12935.

[6] Reece, S. Y.; Hamel, J. A.; Sung, K.; Jarvi, T. D.; Esswein, A. J.; Pijpers, J. J.; Nocera, D. G. Wireless solar water splitting using silicon-based semiconductors and earth-abundant catalysts. *Science* **2011**, 334, 645-648.

[7] McKone, J. R.; Warren, E. L.; Bierman, M. J.; Boettcher, S. W.; Brunschwig, B. S.; Lewis, N. S.; Gray, H. B. Evaluation of Pt, Ni, and Ni–Mo electrocatalysts for hydrogen evolution on crystalline Si electrodes. *Energy Environ. Sci.* **2011**, 4, 3573-3583.

[8] Chen, W. F.; Sasaki, K.; Ma, C.; Frenkel, A. I.; Marinkovic, N.; Muckerman, J. T.; Zhu, Y.; Adzic, R. R. Hydrogen-Evolution Catalysts Based on Non-Noble Metal Nickel-Molybdenum Nitride Nanosheets. *Angew. Chem. Inter. Ed.* **2012**, 51, 6131-6135.

[9] Vrubel, H.; Hu, X. Molybdenum boride and carbide catalyze hydrogen evolution in both acidic and basic solutions. *Angew. Chem. Inter. Ed.* **2012**, 124, 12875-12878.

[10] Chen, W. F.; Wang, C.-H.; Sasaki, K.; Marinkovic, N.; Xu, W.; Muckerman, J.; Zhu, Y.; Adzic, R. Highly active and durable nanostructured molybdenum carbide electrocatalysts for hydrogen production. *Energy Environ. Sci.* **2013**, 6, 943-951.

[11] Jaramillo, T. F.; Jorgensen, K. P.; Bonde, J.; Nielsen, J. H.; Horch, S.; Chorkendorff, I. Identification of active edge sites for electrochemical H_2 evolution from MoS_2 nanocatalysts. *Science* **2007**, 317, 100-102.

[12] Kibsgaard, J.; Chen, Z. B.; Reinecke, B. N.; Jaramillo, T. F. Engineering the surface structure of MoS_2 to preferentially expose active edge sites for electrocatalysis. *Nat. Mater.* **2012**, 11, 963-969.

[13] Merki, D.; Hu, X. Recent developments of molybdenum and tungsten sulfides as hydrogen evolution catalysts. *Energy Environ. Sci.* **2011**, 4, 3878-3888.

[14] Voiry, D.; Yamaguchi, H.; Li, J. W.; Silva, R.; Alves, D. C. B.; Fujita, T.; Chen, M. W.; Asefa, T.; Shenoy, V. B.; Eda, G.; Chhowalla, M. Enhanced catalytic activity in strained chemically exfoliated WS_2 nanosheets for hydrogen evolution. *Nat. Mater.* **2013**, 12, 850-855

[15] Sun, Y.; Liu, C.; Grauer, D. C.; Yano, J.; Long, J. R.; Yang, P.; Chang, C. J. Electrodeposited Cobalt-Sulfide Catalyst for Electrochemical and Photoelectrochemical Hydrogen Generation from Water. *J. Am. Chem. Soc.* **2013**, 135, 17699-17702.

[16] Kong, D.; Cha, J. J.; Wang, H.; Lee, H. R.; Cui, Y. First-row transition metal dichalcogenide catalysts for hydrogen evolution reaction. *Energy Environ. Sci.* **2013**, 6, 3553-3558.

[17] Popczun, E. J.; McKone, J. R.; Read, C. G.; Biacchi, A. J.; Wiltrout, A. M.; Lewis, N. S.; Schaak, R. E. Nanostructured nickel phosphide as an electrocatalyst for the hydrogen evolution reaction. *J. Am. Chem. Soc.* **2013**, 135, 9267-9270.

[18] Yu, Y.; Huang, S.; Li, Y.; Steinmann, S. N.; Yang, W.; Cao, L. Layer-dependent Electrocatalysis of MoS_2 for Hydrogen Evolution. *Nano Lett.* **2014**, 14, 553-558.

[19] Karunadasa, H. I.; Montalvo, E.; Sun, Y. J.; Majda, M.; Long, J. R.; Chang, C. J. A Molecular MoS_2 Edge Site Mimic for Catalytic Hydrogen Generation. *Science* **2012**, 335, 698-702.

[20] Hou, Y. D.; Abrams, B. L.; Vesborg, P. C. K.; Bjorketun, M. E.; Herbst, K.; Bech, L.; Setti, A. M.; Damsgaard, C. D.; Pedersen, T.; Hansen, O.; Rossmeisl, J.; Dahl, S.; Norskov, J. K.; Chorkendorff, I. Bioinspired molecular co-catalysts bonded to a silicon photocathode for solar hydrogen evolution. *Nat. Mater.* **2011**, 10, 434-438.

[21] Hinnemann, B.; Moses, P. G.; Bonde, J.; Jorgensen, K. P.; Nielsen, J. H.; Horch, S.; Chorkendorff, I.; Norskov, J. K. Biornimetic hydrogen evolution: MoS_2 nanoparticles as catalyst for hydrogen evolution. *J. Am. Chem. Soc.* **2005**, 127, 5308-5309.

[22] Norskov, J. K.; Bligaard, T.; Rossmeisl, J.; Christensen, C. H. Towards the computational design of solid catalysts. *Nat.Chem.* **2009**, 1, 37-46.

[23] Zhou, H.; Yu, F.; Liu, Y.; Zou, X.; Cong, C.; Qiu, C.; Yu, T.; Yan, Z.; Shen, X.; Sun, L. Thickness-dependent patterning of MoS_2 sheets with well-oriented triangular pits by heating in air. *Nano Res.* **2013**, 6, 703-711.

[24] Huang, Y.; Wu, J.; Xu, X.; Ho, Y.; Ni, G.; Zou, Q.; Koon, G.; Zhao, W.; Neto, A.; Eda, G. An innovative way of etching MoS_2: Characterization and mechanistic investigation. *Nano Res.* **2013**, 6, 200-207.

[25] Liu, C.; Dasgupta, N. P.; Yang, P. Semiconductor Nanowires for Artificial Photosynthesis. *Chem. Mater.* **2014**, 26, 415-422.

[26] Yang, P.; Yan, R.; Fardy, M. Semiconductor nanowire: what's next? *Nano Lett.* **2010**, 10, 1529-1536.

[27] Boettcher, S. W.; Spurgeon, J. M.; Putnam, M. C.; Warren, E. L.; Turner-Evans, D. B.; Kelzenberg, M. D.; Maiolo, J. R.; Atwater, H. A.; Lewis, N. S. Energy-conversion properties of vapor-liquid-solid-grown silicon wire-array photocathodes. *Science* **2010**, 327, 185-187.

[28] Seger, B.; Pedersen, T.; Laursen, A. B.; Vesborg, P. C.; Hansen, O.; Chorkendorff, I. Using TiO_2 as a conductive protective layer for photocathodic H_2 evolution. *J. Am. Chem. Soc.* **2013**, 135, 1057-1064.
[29] Brito, J. L.; Ilija, M.; Hernández, P. Thermal and reductive decomposition of ammonium thiomolybdates. *Thermochim. Acta* **1995**, 256, 325-338.
[30] Liu, K. K.; Zhang, W.; Lee, Y. H.; Lin, Y. C.; Chang, M. T.; Su, C. Y.; Chang, C. S.; Li, H.; Shi, Y.; Zhang, H.; Lai, C. S.; Li, L. J. Growth of large-area and highly crystalline MoS_2 thin layers on insulating substrates. *Nano Lett.* **2012**, 12, 1538-1544.
[31]Tributsch, H.; Bennett, J. Electrochemistry and photochemistry of MoS_2 layer crystals. *J. Electroanal. Chem.* **1977**, 81, 97-111.
[32] Gomez, A.; van der Zant, H.; Steele, G. Folded MoS_2 layers with reduced interlayer coupling. *Nano Res.* **2014**, 7, 1-7.
[33] Seger, B.; Laursen, A. B.; Vesborg, P. C.; Pedersen, T.; Hansen, O.; Dahl, S.; Chorkendorff, I. Hydrogen production using a molybdenum sulfide catalyst on a titanium-protected n^+p-silicon photocathode. *Angew Chem. Int. Ed.* **2012**, 5, 9128-9131.
[34] Kong, D.; Wang, H.; Cha, J. J.; Pasta, M.; Koski, K. J.; Yao, J.; Cui, Y. Synthesis of MoS_2 and $MoSe_2$ Films with Vertically Aligned Layers. *Nano Lett.* **2013**, 13, 1341-1347.

Electronic Supplementary Material

MoS_2-wrapped silicon nanowires for photoelectro-chemical water reduction

Liming Zhang[1,†,§], Chong Liu[1,§], Andrew Barnabas Wong[1,4], Joaquin Resasco[2], and Peidong Yang[1,3,4] (✉)

[1]*Department of Chemistry,* [2]*Department of Chemical Engineering and* [3]*Department of Materials Science and Engineering, University of California, Berkeley, CA 94720, United States*

[4]*Materials Science Division, Lawrence Berkeley National Laboratory, Berkeley, CA 94720, United States*

[†]*Present address: Department of Materials Science and Engineering, Stanford University, Stanford, CA 94305, USA*

[§]*These authors contributed equally to this work.*

Supporting information to DOI 10.1007/s12274-****-****-*

Nanowire (NW) Array Synthesis: The well-defined periodic Silicon (Si) NW arrays (Figure 3c-d) were fabricated using reactive-ion etching of patterned single-crystalline Si wafers. P-type boron-doped 4" Si wafers (<100> oriented, 0.1~0.2 Ω cm) were first patterned with a photo-resist dot array using a standard photolithography stepper. Then the wafer underwent inductive-coupled plasma deep reactive-ion etching (Surface Technology Systems, Inc.) to produce NW arrays with uniform diameter ~850 nm and length ~30 μm. After removing the residual photo-resist by an O_2 plasma, 50 nm of dry thermal oxide was grown on the NWs at 1050 ℃ for 40 min. After a 5:1 buffered HF etch and critical point drying (Tousimis, Inc.), Si NW arrays with wires whose diameters were about 800 nm were obtained.

Atomic Layer Deposition (ALD) of TiO_2: The deposition procedure was developed based on the previous reported method [1]. Si NWs array samples were etched in 1:10 HF buffer solution for 1 min, and cleaned with DI water and isopropyl alcohol, followed by rapid drying on a hot plate at a temperature of 90 ℃. This fast drying method helps to maintain the vertical morphology of NW array. TiO_2 shells were deposited on Si NW array by using a custom built ALD system at 300 ℃ with $TiCl_4$ (99.99% , Alfa) and pure DI water as the precursors. The deposition rate was ~0.5 Å/cycle.

Low temperature annealing of MoS_2: The MoS_2 cocatalyst was synthesized on the surface of NWs by thermal annealing of molybdenum precursor, $(NH_4)_2MoS_4$, under reducing atmosphere. $(NH_4)_2MoS_4$ powder (Alfa Asear, purity of 99.99%, 0.125 g) was dissolved into methanol/Hexamethyldisilazane (HMDS) solution (10 ml/20 μl) under magnetic agitation to fully disperse the powder. The low surface tension solvent HMDS (18.2 mN/m at 293 K) was used to preserve the morphology of the NW array. The solution was drop-casted onto the NW surface. The

drop-casting volume depends on the density (roughness factor) of the NW array and the projected area of Si substrate. For example, for a 1 cm×1 cm Si substrate with a NW array with surface roughness factor 30, the optimal volume was 25 μl. A glass dish cap was used to cover the substrate to allow for slow evaporation of the methanol. MoS_2 layers were obtained by annealing the precursor at 300~400℃ in a N_2/H_2 (80/20 sccm) atmosphere at ambient pressure for 2 h.

Transmission Electron Microscopy (TEM): Electron microscopy was performed at the National Center for Electron Microscopy in Lawrence Berkeley National Lab. TEM images were taken at 200 kV on a FEI Tecnai F20 microscope with an ultra-twin lens. High-angle annular dark-field (HAADF) images and energy dispersive X-ray spectroscopy (EDS) maps were acquired using a FEI Titan microscope operated at 80 kV. The microscope was equipped with a Fischione HAADF detector that had inner semi-angle of 79 mrad. EDS mapping images were acquired using a FEI Super-X Quad windowless detector based on silicon drift technology and processed using Bruker Esprit software, which was calibrated against mineral standards for quantitative accuracy.

X-ray Photoelectron Spectroscopy (XPS) and Raman spectroscopy: XPS spectra were collected using a PHI 5400 X-ray Photoelectron Spectrometer equipped with a 4 kV Argon ion gun, with Al K radiation. The angle between the source and detector was 35°. The measurement chamber was maintained at 10^{-9} eV during measurement, and measurements were taken at a pass energy of 17.9 eV. All energies were calibrated to spurious carbon at 285.0 eV. Raman spectroscopy was taken by a Horiba HR800 system with laser excitation energy of 532 nm. The laser spot size is ~1 μm and a laser power of ~5 mW was used to avoid heating.

Photoelectrochemistry (PEC) measurements: Electrochemical and photoelectrochemical measurements of electrodes were performed using a Biologic potentiostat. All measurements were performed under purged Ar gas environment and in a 0.5 M sulfuric acid electrolyte (pH = 0.48). Ag/AgCl in 1 M NaCl (CHI, Corp.) was used as a reference electrode when needed, and all voltages reported were calculated versus the reversible hydrogen electrode (RHE) using the following equation:

$$V \text{ vs RHE (volt)} = \text{V vs Ag/AgCl (volt)} + 0.234 \text{ (volt)} + 0.0591 \times pH$$

The light source used for simulated sunlight in this report was a 300-Watt xenon lamp equipped with an air mass 1.5G filter (Newport). Before each measurement, a calibrated silicon photodiode determined the light intensity at the position of the electrode being measured. The J-V photocurrent data for individual photoelectrodes were measured using a standard three-electrode setup under simulated one-sun illumination, with a scan rate of 10 mV/sec. The dark currents were orders of magnitude lower than photocurrent in all cases within the voltage ranges measured. For the incident photon to current conversion efficiency (IPCE) measurement, a 300 W Xe lamp was coupled with a monochromator (Newport, cornerstone 130), and the incident light intensity was measured with a calibrated Si photodiode. Here, the IPCE was calculated from the photocurrents measured at -0.33 V vs. RHE, according to the following equation:

$$\mathbf{IPCE} = \frac{\mathbf{I_{ph}}\left(\frac{\mathbf{mA}}{\mathbf{cm^2}}\right) \times \mathbf{1239.8\,(V \times nm)}}{\mathbf{P_{mono}}\left(\frac{\mathbf{mW}}{\mathbf{cm^2}}\right) \times \boldsymbol{\lambda}\mathbf{(nm)}}$$

Determination of Faradaic efficiency: The experiment was conducted in a sealed cell containing 0.5 M H_2SO_4 electrolyte through which Ar carrier gas was flowed at a rate of 5 sccm. Controlled potential electrolysis were conducted at an applied potential of –0.33 V vs RHE for 75 min. Figure S5 shows the generated hydrogen volume during photoelectrolysis in sulfuric acid based on a gas chromatography (Varian Micro-GC with a Molecular Sieve 5Å column, 40 m) measurement.

Precursor loading volume (μl)	MoS_2 loading amount[a] (10^{-7} mol/cm^2)	j_0[b] (10^{-8}A/cm^2)	Tafel slope[c] (mV/dec)
1.0	0.48	2.62 ±0.12	74.7 ±0.4
2.5	1.2	4.15 ±0.14	74.8 ±0.3
5.0	2.4	8.97 ±0.21	78.6 ±0.3
10	4.8	23.6 ±0.7	84.2 ±0.5

Table S1. Calculation of the electrochemical performance of MoS_2. [a] The absolute loading amount of MoS_2 is calculated based on the concentration and loading volume of precursor. [b] j_0 exchange current density and [c] Tafel slope were calculated from Tafel plots in Figure 3b.

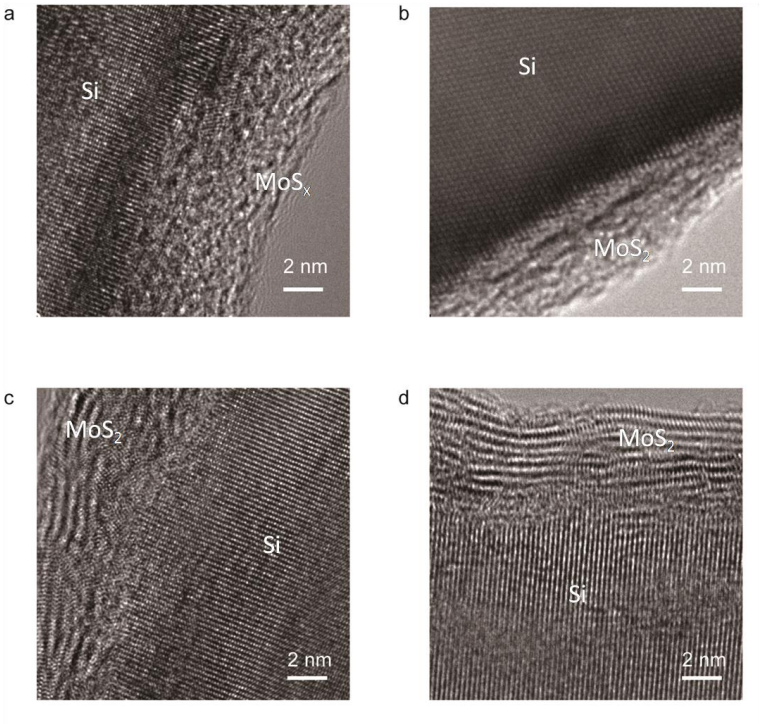

Figure S1. High resolution TEM images of MoS_x on NW without annealing (a) and at different annealing temperature (b) 200 ℃; (c) 300 ℃ and (d) 400 ℃. The crystallinity of MoS_2 highly depends on the annealing temperature, with increasing temperature resulting in higher crystallinity.

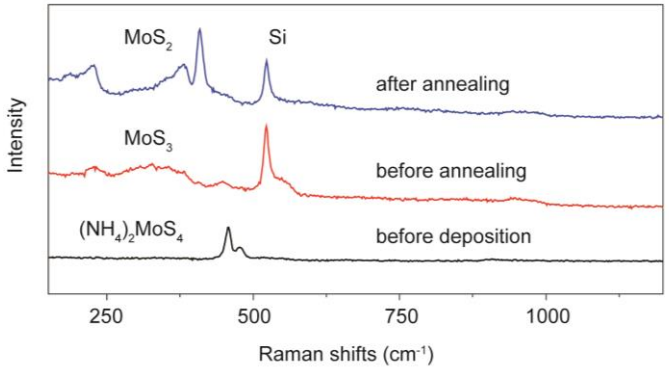

Figure S2. Raman spectra evolution of cocatalysts before and after thermal annealing. The peak at ~383 and 407 cm^{-1} demonstrates the formation of MoS_2.

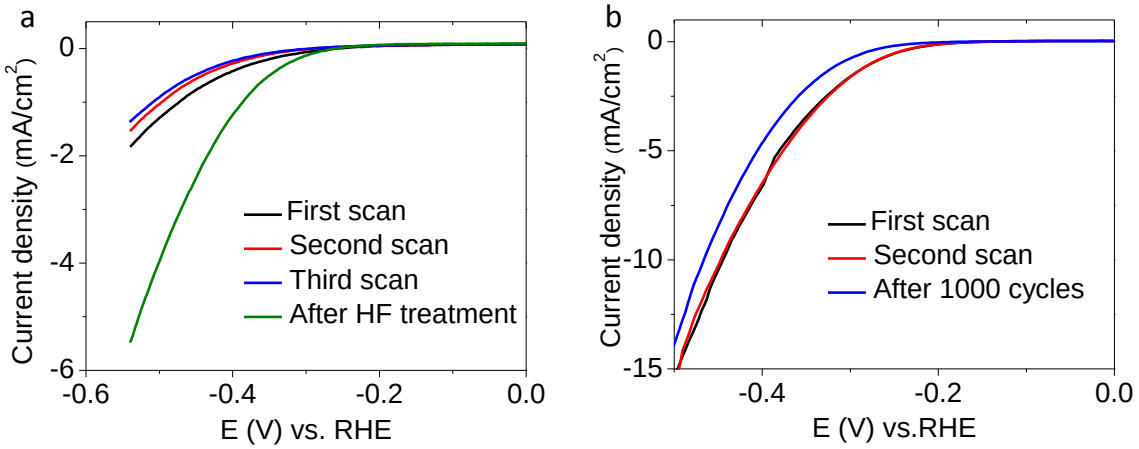

Figure S3. Linear sweep voltammograms for (a) p^+Si and (b) TiO_2/p^+ Si planar surface coated with MoS_2 cocatalyst. The performance recovery after HF treatment in (a) indicates the oxidation of Si is the main cause for the performance degradation.

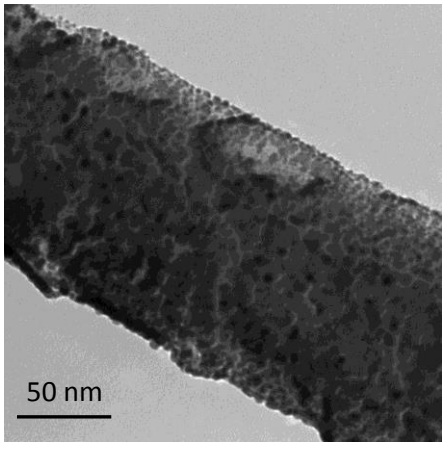

Figure S4. TEM image of a Pt nanoparticle coated TiO_2/Si NW.

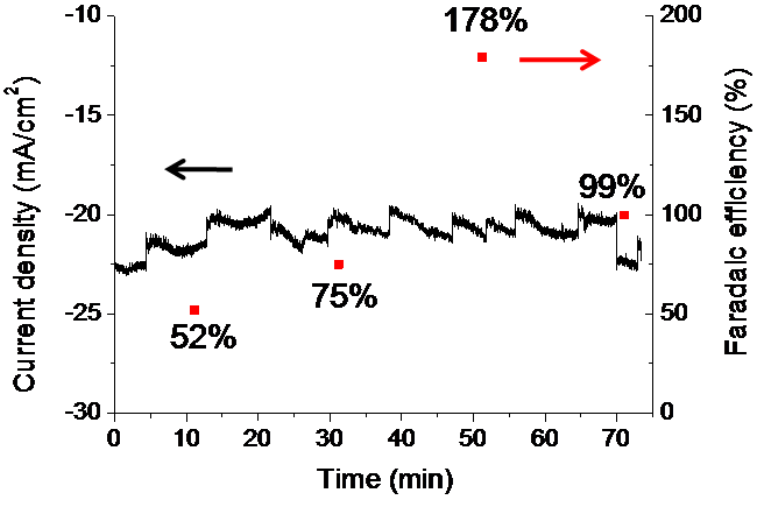

Figure S5. Chronoamperometry measurement of $MoS_2/TiO_2/n^+p$-Si NW array held at a constant potential of -0.33 V vs. RHE under 1 sun illumination. Bubbles were continuously evolved from photocathode, and the accumulation and release of these bubbles led to the observed variations in photocurrent over the duration of the measurement. The large variation of faradaic efficiency originated from the accumulation of hydrogen bubble on the electrode surface. The average faradaic efficiency calculated in the 75 min time range is ~100%.

Reference:

(1) Hwang, Y. J.; Hahn, C.; Liu, B.; Yang, P. *ACS Nano* **2012**, *6*, 5060.

Address correspondence to p_yang@berkeley.edu